GEOLOGICAL SURVEY OF CANADA
OPEN FILE 7852

# Targeted Geoscience Initiative 4: Contributions to the Understanding of Precambrian Lode Gold Deposits and Implications for Exploration

## Genesis of the Canadian Malartic, Côté Gold, and Musselwhite gold deposits: Insights from LA-ICP-MS element mapping of pyrite

**Jian-Feng Gao[1], Simon E. Jackson[1], Benoît Dubé[2], Daniel J. Kontak[3], and Stéphane De Souza[2]**

[1]Geological Survey of Canada, Ottawa, Ontario
[2]Geological Survey of Canada, Québec, Quebec
[3]Laurentian University, Sudbury, Ontario

**2015**



This publication is available for free download through GEOSCAN (http://geoscan.nrcan.gc.ca/)

**Recommended citation**

Gao, J.-F., Jackson, S.E., Dubé, B., Kontak, D.J., and De Souza, S., 2015. Genesis of the Canadian Malartic, Côté Gold, and Musselwhite gold deposits: Insights from LA-ICP-MS element mapping of pyrite, *In:* Targeted Geoscience Initiative 4: Contributions to the Understanding of Precambrian Lode Gold Deposits and Implications for Exploration, (ed.) B. Dubé and P. Mercier-Langevin; Geological Survey of Canada, Open File 7852, p. 157–175.

Publications in this series have not been edited; they are released as submitted by the author.

**Contribution to the Geological Survey of Canada's Targeted Geoscience Initiative 4 (TGI-4) Program (2010–2015)**

## TABLE OF CONTENTS

# Genesis of the Canadian Malartic, Côté Gold, and Musselwhite gold deposits: Insights from LA-ICP-MS element mapping of pyrite

Jian-Feng Gao[1], Simon E. Jackson*, Benoît Dubé[2], Daniel J. Kontak[3], and Stéphane De Souza[2]

[1]Geological Survey of Canada, 601 Booth Street, Ottawa, Ontario K1A 0E9
[2]Geological Survey of Canada, 490 rue de la Couronne, Québec, Quebec G1K 9A9
[3]Department of Earth Sciences, Laurentian University, Sudbury, Ontario P3E 2C6
*Corresponding author's e-mail: Simon.Jackson@NRCan-RNCan.gc.ca

## ABSTRACT

Pyrite efficiently incorporates many key metals during progressive precipitation and thus records the chemical evolution of fluids from which it was deposited. To reveal this information, a new LA-ICP-MS mapping procedure has been developed to allow generation of 2-D trace element concentration maps of minerals in petrographic section. The technique has been applied to pyrite-/pyrrhotite-bearing Au ores from three major gold deposits.

Canadian Malartic is a low-grade bulk-tonnage deposit, which is located immediately south of the Larder Lake–Cadillac Fault Zone. It is hosted mainly by clastic metasedimentary rocks of the Pontiac Group, as well as by porphyritic quartz monzodiorite and granodiorite. Textural evidence and elemental mapping have revealed five types of pyrite. The pre-mineralization pyrite (py1) is likely diagenetic pyrite, with high Co, As, and Se, and low Ni, Te, Sb, Bi, and Pb. Gold-bearing pyrite 2, 3 and 4 (py2–py4) has covariant Co and Ni, high Au, Ag, Te, Bi, and Pb, and generally contains abundant potassic inclusions. Post-mineralization pyrite (py5) has high Co and Ni but is low in other metals. Pyrite from the ore zones distributed along the Sladen fault zone shows evidence of post-precipitation metal enrichment in fractures associated with Ca metasomatism. Though the elemental maps cannot unequivocally discriminate the deposit type, pyrite chemistry is consistent with a two-stage model comprising early syn-pyrite Au mineralization associated with potassium alteration and a later post-pyrite upgrading associated with Ca metasomatism.

The Côté Gold deposit is hosted by the Chester intrusive complex, a high-level, multi-phase synvolcanic intrusion composed of tonalite and diorite. Nickel, As, Sb, and Pb are generally relatively depleted in the cores and enriched in the rims of the pyrite grains, whereas Te and Ag are relatively enriched in the cores and depleted in the rims. Arsenopyrite grains have high Co, Ni, Se, Sb, and Te, but low Ag, Pb, and Bi. Gold is depleted both in pyrite and arsenopyrite, except locally in fractures, but is enriched in silicate minerals, possibly as nanoparticles, suggesting that gold mineralization is related to a hydrothermal event post-dating pyrite precipitation.

The Musselwhite deposit is a banded iron formation-hosted lode gold deposit in a sequence of volcanic and sedimentary rocks that include carbonaceous argillite locally hosting diagenetic pyrite nodules. Cobalt, Cu, Ni, Se, As, Ag, Sb, Te, Au, Tl, Pb, and Bi are enriched in the nodules but are depleted in recrystallized pyrite and pyrrhotite. Element and Pb-isotope maps are consistent with a model whereby at least some of the ore gold was derived from fluids that garnered Au liberated via metamorphic recrystallization of auriferous diagenetic pyrite and, probably, carbonaceous material in local argillite.

The elemental maps show that gold has multiple sources. The Musselwhite deposit provides evidence for local pyritic carbonaceous sedimentary rocks as one of the possible sources of Au. The Canadian Malartic and Côté deposits have a strong association with magmatic hydrothermal activity, although additional sources of Au may also have been important.

## INTRODUCTION

Gold in ores may be visible or it may occur as so called "invisible gold" (Cook and Chryssoulis, 1990), either lattice-bound in sulphides or as nanoparticle inclusions (Deditius et al., 2011; Hough et al., 2011; Cook et al., 2013). Gold can partition into sulphide minerals during precipitation, or can be released from a sulphide lattice during later deformation, metamorphism, and recrystallization (Large et al., 2007, 2009). Cobalt and Ni can substitute for Fe in pyrite, whereas As, Se, and Te are likely to exchange with S in the pyrite lattice. Pyrite crystallized from fluids/melts with different Co, Ni, As,

Gao, J.-F., Jackson, S.E., Dubé, B., Kontak, D.J., and De Souza, S., 2015. Genesis of the Canadian Malartic, Côté Gold, and Musselwhite gold deposits: Insights from LA-ICP-MS element mapping of pyrite, *In:* Targeted Geoscience Initiative 4: Contributions to the Understanding of Precambrian Lode Gold Deposits and Implications for Exploration, (ed.) B. Dubé and P. Mercier-Langevin; Geological Survey of Canada, Open File 7852, p. 157–175.

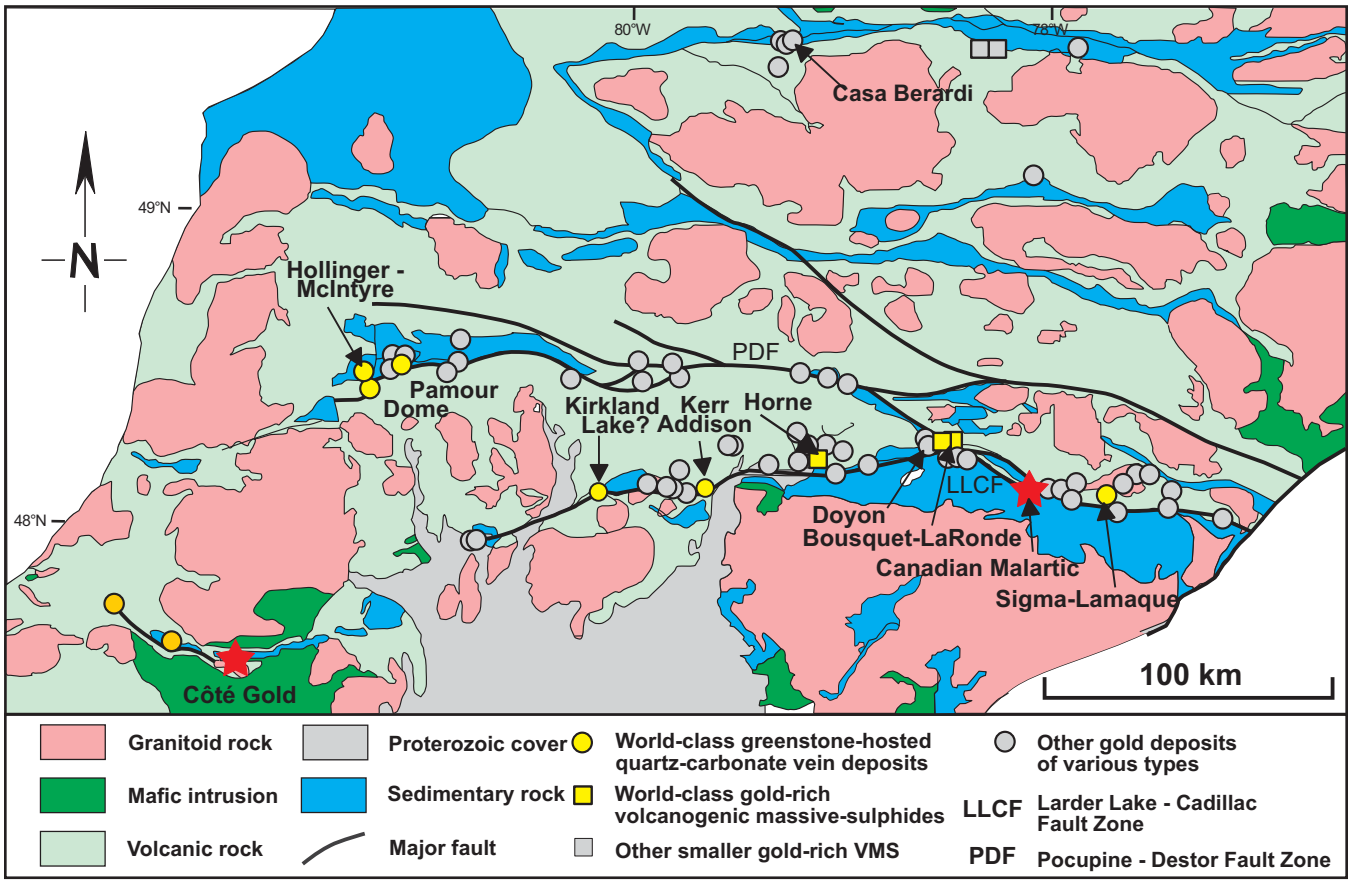


**Figure 1.** Simplified geological map of the Abitibi greenstone belt showing the distribution of major fault zones and gold deposits. Modified from Poulson et al. (2000) and Dubé and Gosselin (2007).

Se, and Te contents will contain different concentrations of these elements (Large et al., 2009; Koglin et al., 2010). Gold has similar geochemical characteristics to trace elements, such as Ag, As, Cu, Se, and Te, during pyrite precipitation but may show behaviour different to these elements during evolution of hydrothermal fluids (Chouinard et al., 2005; Large et al., 2009). In addition, previous studies on elemental distributions in pyrite have illustrated that it can contain highly variable contents of trace elements at the grain scale and that Au contents can correlate with different elements in different zones of a pyrite grain (Chouinard et al., 2005; Large et al., 2009; Deol et al., 2012; Agangi et al., 2013; Cook et al., 2013; Large et al., 2013). Thus, the textural and chemical differences among the pyrite grains have tremendous potential for providing information about the processes of gold mineralization (Koglin et al., 2010).

The Abitibi greenstone belt is a 750 km-long by 200 km-wide belt of metamorphosed volcanic, coeval subvolcanic, and intrusive rocks, locally derived clastic and chemical sedimentary rocks, and granitoid batholiths. It is the largest greenstone belt in the world and hosts world-class gold deposits of various styles, including greenstone-hosted quartz-carbonate Au vein, Au-rich VMS, syenite-associated disseminated gold, and intrusion-related deposits (Hodgson and McGeehan, 1982; Robert et al., 2005; Dubé and Gosselin, 2007, Dubé et al., 2007; Mercier-Langevin et al., 2007). Pyrite is the most common sulphide mineral in many of the gold ore assemblages. Due to different formation conditions in these various types of deposits, pyrite may have different morphologies and trace chemical compositions, which can record the paleofluid chemistry during its crystallization history.

In this study, we present new elemental maps of different types of pyrite from three gold deposits, including the intrusion-related stockwork-disseminated Canadian Malartic (Québec) and Côté Gold (Ontario) deposits located, respectively, in the Abitibi and Swayze greenstone belts, Abitibi Subprovince (Fig. 1), and the Musselwhite deposit (Ontario) of the North Caribou greenstone belt. Our aim is to combine these new data sets with detailed field mapping to help constrain the processes of gold mineralization in these deposits. This study demonstrates that quantitative elemental mapping of different generations of pyrite is a very powerful tool for interrogating minerals for the processes and physico-chemical evolution of their host hydrothermal systems and addressing the source(s) of

gold. This information can further our understanding of gold mineralizing processes and can be applied in gold exploration to vector toward potential ore zones.

## RESULTS

### Methodology

The application of LA-ICP-MS to 2-D trace element mapping of geological minerals has grown rapidly since its tremendous potential was first highlighted (Woodhead et al., 2007, 2008). However, because of calibration difficulties, most published examples have presented either signal intensity maps, or concentration maps of single mineral phases. For this study, 2-D element concentration maps of multi-phase mineral assemblages were required to allow quantitative interpretation of the distributions of Au and other elements. Additionally, because of the generally small grain size of hydrothermal minerals, methods were sought to improve the sampling resolution obtainable using the traditional line-scan sampling approach to LA-ICP-MS mapping (Woodhead et al., 2007, 2008), where constant sample stage translation and ablation aerosol mixing degrades resolution.

Firstly, the area mapped was sampled via thousands of discrete edge-to-edge square ablation spots. While collecting signal intensities for about 40 elements (typically, C, Na, Mg, Al, Si, P, S, K, Ca, Ti, V, Cr, Mn, Fe, Co, Ni, Cu, Zn, As, Se, Mo, Ag, Sb, Te, Ba, La, W, Au, Hg, Tl, Pb, Bi, U, plus about 5–7 of B, Ga, Sr, Zr, In, Sn, Cs, Ce, Nd, Sm, Gd, Yb, Lu, Th), each spot was in turn "pre-ablated" (3–5 laser pulses) to remove surface contaminants resulting from polishing and sample fallback from neighbouring spots. This material was flushed from the system (1.5 s) prior to ablation (2 s). The protocol was repeated until the entire selected area was sampled. The major advantage of this sampling protocol is that it produces true spot-size limited sampling resolution. It also removes surface contamination at each sampling site immediately prior to analysis.

To allow quantification of multi-phase mineral assemblages, standardization was achieved via external calibration against United States Geological Survey (USGS) synthetic basaltic glass reference material GSE-1G, coupled with ablation yield correction via normalization to 100% total element abundance (Halicz and Günther, 2004), performed on a spot-by-spot basis. To extend the calibration to S and C, which are not present in GSE-1G, surrogate calibration was applied using S/Fe and C/Ca sensitivity ratios determined by ablation of pure pyrrhotite and calcite, respectively. The methodology outlined above provides quantitative analysis without prior knowledge and input of internal standard element concentrations for each ablation spot and it is the most appropriate approach to calculating concentrations for spots that sample more than one mineral phase (e.g. small inclusions, grain boundaries). Lead isotope maps were also generated but in separate analytical sessions using a much reduced element list and calibration against GSE-1G.

Algorithms and software were developed to selectively integrate the ablation signals produced by each ablation spot and calculate concentrations via external standardization and internal normalization to 100%, including deconvolution calculations to determine, for each spot, O (and H) contents, which cannot be measured. The latter is complicated particularly by Fe, which may be present, in any ablation volume, as FeO and/or $Fe_2O_3$ and/or a Fe sulphide. The above was achieved by modification and full automation of in-house spreadsheet software, LAMTrace (Jackson, 2008) and its sister program, Convert (the latter subsequently rewritten as a VBA-driven Microsoft Excel® program). Another spreadsheet program (PixeLAte) was written to generate element concentration maps by displaying element concentrations for each spot as coloured pixels using a choice of colour schemes and scaling functions. A percentile scaling function is generally employed for displaying maps of low-abundance elements because it most effectively highlights subtle concentration differences. A logarithmic scaling function is generally employed for displaying more homogeneously distributed elements (e.g. major elements). A function was written that allows users to interrogate selected areas of the maps for statistical calculations of the values in the area selected (i.e. n, mean, median, standard deviation, standard error, relative standard deviation and relative standard error).

### Canadian Malartic

The Canadian Malartic gold deposit, Val d'Or, Québec, is mainly hosted (~75%) in altered clastic (turbiditic) metasedimentary rocks of the Pontiac Group and in subalkaline porphyritic quartz monzodiorite and granodiorite located immediately south of the Larder Lake–Cadillac Fault Zone (De Souza et al., 2015, in press). Mineralization also occurs in dykes and sills of various compositions, but porphyritic quartz monzodiorite represents the main mineralized intrusive phase. The rocks have been deformed and metamorphosed to upper greenschist facies. Mineralization is distributed according to two main trends, forming east-west and northwest-southeast-trending ore zones (De Souza et al., 2015, in press). At the surface, the dominant east-west trend coincides with the position of the Sladen Fault and gold is hosted by quartz monzodiorite and by metasedimentary rocks along and adjacent to the fault zone. The surface trace of the northwest-southeast mineralized trend is subparallel to the $S_2$ cleavage, which is axial planar to $F_2$ folds. Though the Canadian

Malartic deposit shows some features suggestive of an intrusion-related deposit, including disseminated and stockwork mineralization associated with potassic alteration, the gold mineralization and its distribution are largely controlled by $D_2$ deformation structures, including faults, shear- and high-strain zones developed in the hinge zone of $F_2$ folds, and by the Sladen Fault. Some of the highest grade mineralization occurs along the Sladen Fault, which cuts the quartz monzodiorite and represents the main gold-bearing structure that was mined during the historical production at the Canadian Malartic, Sladen, and East Malartic mines (De Souza et al., 2015). The aim of this study is to determine whether element mapping of pyrite can shed any light on the origin(s) of the gold at Canadian Malartic.

Based on morphological and textural features, pyrite in the Canadian Malartic gold deposit can be subdivided into five types, which we refer to as py1 to py5. Element distributions in different types of pyrite are shown in Figures 2 to 5. Pyrite py1 is porous and has high Co, As, Se, but low Ni, Te, Sb, and Au concentrations and dominantly Ca-bearing inclusions. Pyrite py2, having sharp boundary with py1, features concentrically zoned, relatively K-rich inclusion trails and has similar Co contents as py1, but shows significant enrichment of Ni, Te, Sb Pb, and Au, and low As and Se contents (Fig. 2). Pyrite py3, containing abundant fine-grained inclusions, has transitional contacts with py1 and is characterized by relatively high Ag, Sb, Pb, and Au contents, low As, Co, and Ni contents, and is locally enriched in Cu (Fig. 3). It is noted that Zn, Mo, Tl, Ag, and Au, together with B, $K_2O$ and $SiO_2$, are concentrated at the rim of some py3 grains. Pyrite py4 is characterized by large inclusions, again dominantly K-rich, and variable Co-Ni-Zn-Sb-Pb-Bi enrichment in the cores and depletion in the rims (Fig. 4). Py4 grains have relatively uniform As (~10 ppm), Se (~5 ppm), Te (~40 ppm), Mo (<0.1 ppm), and Tl (<0.1 ppm) concentrations and relatively high but variable Ag (~10 ppm) and Au (~2 ppm) concentrations. Pyrite py5, which occurs as inclusion-free rims to py1–py4, generally has high Co, Ni, and Se, and low As, Te, and Sb content. In general, it is extremely depleted in Cu, Au, Tl, Pb, and Bi (Figs. 3–5).

Pyrite from the Sladen zone (Fig. 5) shows late, post-pyrite-deposition fracturing. The fractures show enhanced concentrations of As, Mo, Ag, Sb, Te, Au, Pb, and Bi, accompanied by significant Ca- but not K-enrichment.

## Côté Gold

The Côté Gold deposit, located in the Chester and Neville townships, occurs within the Swayze greenstone belt, to the southwest of the Abitibi greenstone belt. The Swayze belt contains a diversity of extrusive and intrusive igneous rock types, ranging in composition from ultramafic to felsic, as well as both chemical and clastic sedimentary rocks. These rocks underwent a complex and protracted history of metamorphism, folding, and development of ductile high-strain zones and late brittle faulting (Heather and van Breemen, 1994; Heather et al., 1996; Heather and Shore 1999a,b; Heather, 2001).

The Côté Gold deposit is hosted by the Chester intrusive complex (CIC), a high-level, multi-phase syn-volcanic intrusion composed of tonalite and diorite, and consists of low- to moderate-grade Au±Cu mineralization (Katz et al., 2015). The mineralized system is centred on a magmatic-hydrothermal breccia body overprinted by several alteration types (biotite, sericite, silica-sodic) (Katz et al., 2015). The overlap of Re-Os dates on syn-gold-deposition molybdenite with the age of the CIC, combined with stable isotopic data (S, O) and field relationships suggest that the deposit is a ca. 2,740 Ma intrusion-related Au(±Cu) deposit (Kontak et al., 2013; Katz et al., 2015). The aim of this study is to determine whether element mapping of pyrite could add new information about the origin(s) of the Côté Gold deposit.

Elemental maps of pyrite from the Côté Gold deposit (n=4) are presented in Figure 6. The study reveals that pyrite from the deposit is characterized by relatively homogeneous Co (>150 ppm), Se (>15 ppm), and Bi (>2 ppm) contents, but highly variable Ni, As, Sb, Te, and Ag contents. The arsenopyrite grain has a relatively homogeneous composition with high Co (>400 ppm), Ni (>200 ppm), Se (>20 ppm), Sb (>8 ppm), and Te (>1 ppm) but low Ag (<0.1 ppm), Au (<0.1 ppm), Pb (<2 ppm) and Bi (<0.3 ppm). Silver and Bi show slight enrichment in the rim of the arsenopyrite grain. Notably, Ag and Au content is extremely poor in pyrite and arsenopyrite grains (<0.1 ppm and <0.14 ppm, respectively), except locally in fractures. However, in three of the four samples mapped, gold is variably enriched (mostly >0.5 ppm) in silicate minerals (biotite, chlorite, and quartz).

## Musselwhite

The Musselwhite gold deposit is located within the North Caribou Greenstone Belt of northwestern Ontario. The stratigraphy in the immediate vicinity of the mine is dominated by mafic and ultramafic volcanic rocks, banded iron formation, felsic volcanic rocks, siliciclastic sedimentary rocks (Biczok et al., 2012; Oswald et al., 2015), and local argillaceous units bearing diagenetic pyrite nodules that range up to >1 cm in diameter. All units in the immediate mine area have been deformed and metamorphosed at amphibolite facies. The bulk of the Au at Musselwhite is hosted

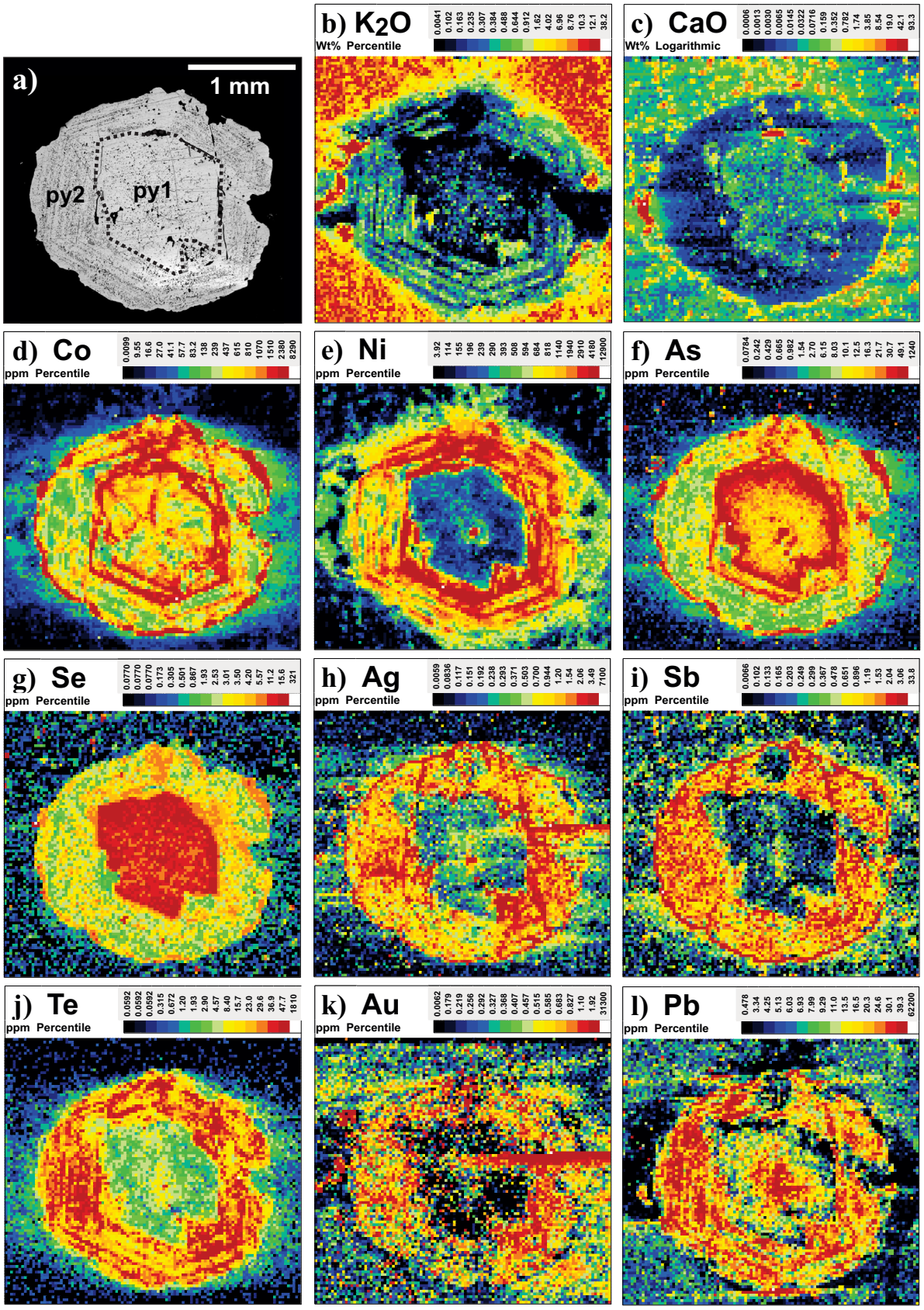


**Figure 2.** Photomicrograph and element concentration maps for pyrite from gold ore (sample CM7) in altered Pontiac sedimentary rocks from the A zone of the Canadian Malartic gold deposit. Scales are in ppm, with the exception of $K_2O$ and CaO, which are in weight percent. The mapped pyrite is composed of py1 and py2. Note the calcic composition of the inclusions in py1 and the relatively potassic composition in py2.

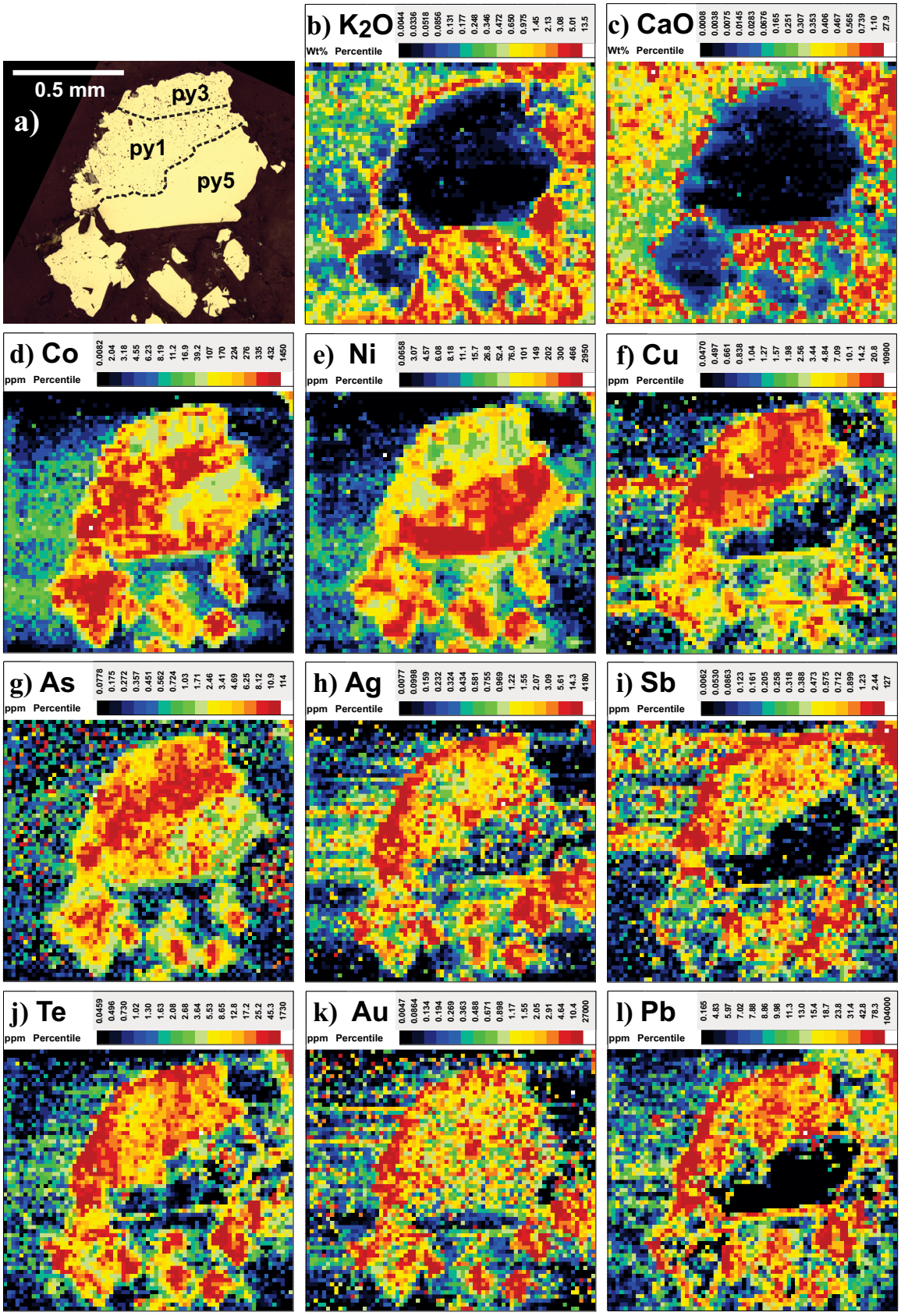


**Figure 3.** Photomicrograph and element concentration maps for pyrite from gold ore (sample CM6) in altered Pontiac sedimentary rocks from the A zone of the Canadian Malartic gold deposit. Scales are in ppm, with the exception of $K_2O$ and CaO, which are in weight percent. The mapped pyrite consists of py1, py3, and py5.

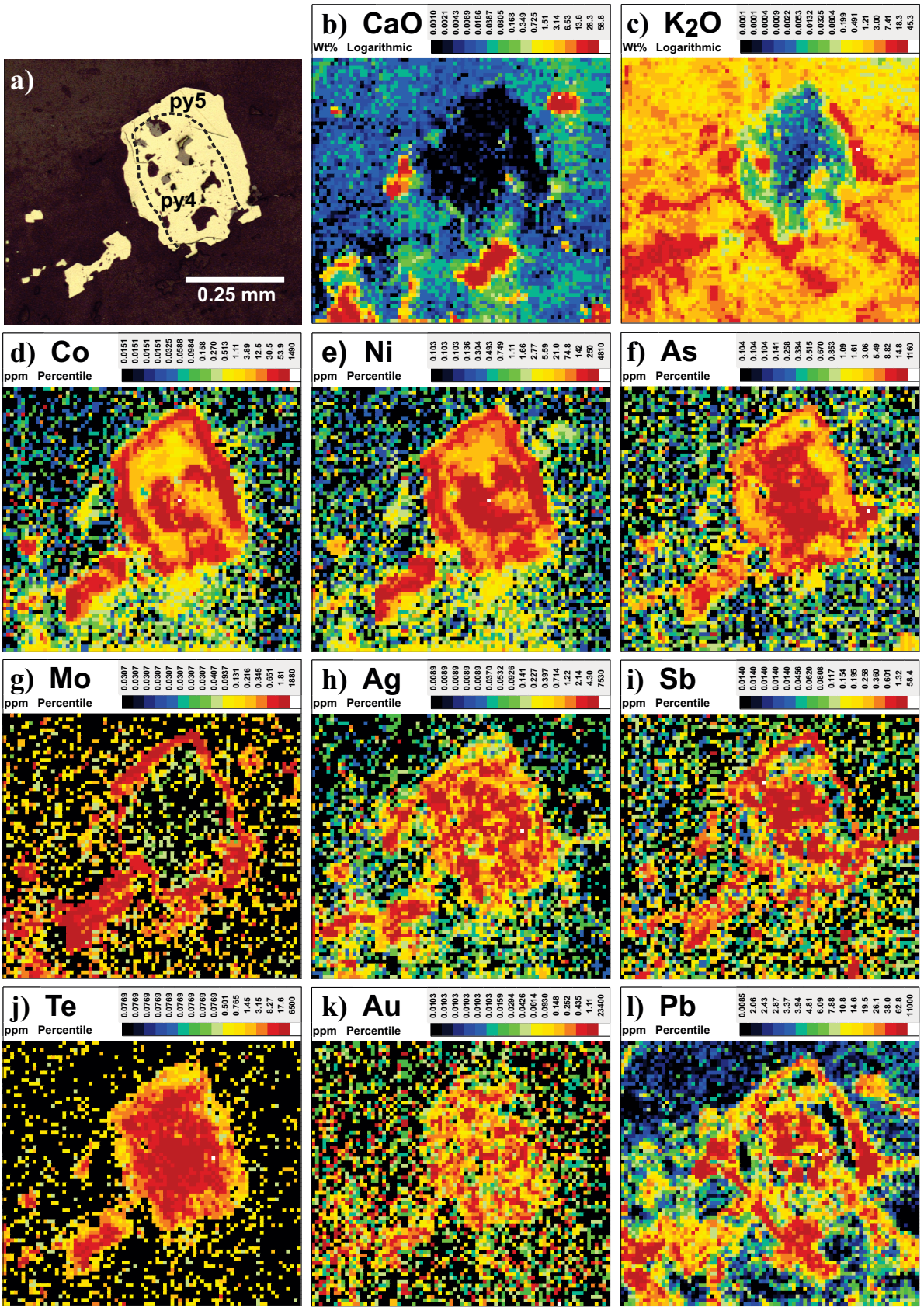


**Figure 4.** Photomicrograph and element concentration maps for pyrite from gold ore (sample CM17) in porphyry rocks of the Sladen zone, Canadian Malartic gold deposit. Scales are in ppm with the exception of $K_2O$ and CaO, which are in weight percent. The mapped pyrite consists of py4 and py5. Note the potassic composition of the large inclusions in py4 and the matrix.

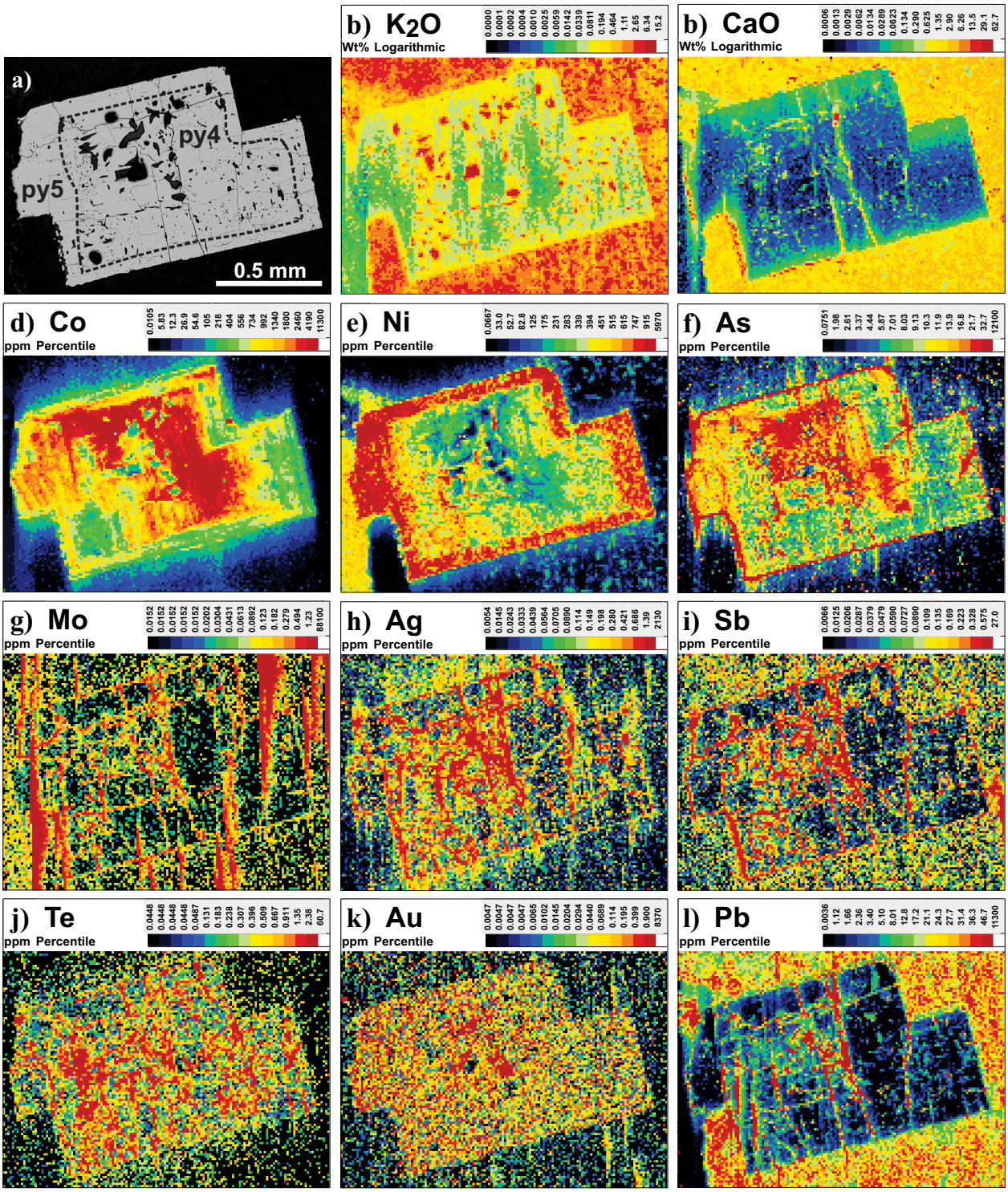


**Figure 5.** Photomicrograph and element concentration maps for pyrite from gold ore (sample CM25) in altered Pontiac sedimentary rocks from the Sladen zone, Canadian Malartic gold deposit. Scales are in ppm, with the exception of $K_2O$ and CaO, which are in weight percent. The mapped pyrite shows late fracturing with metal and Ca enrichments along fractures, perhaps representing post-magmatic, structurally related hydrothermal overprinting.

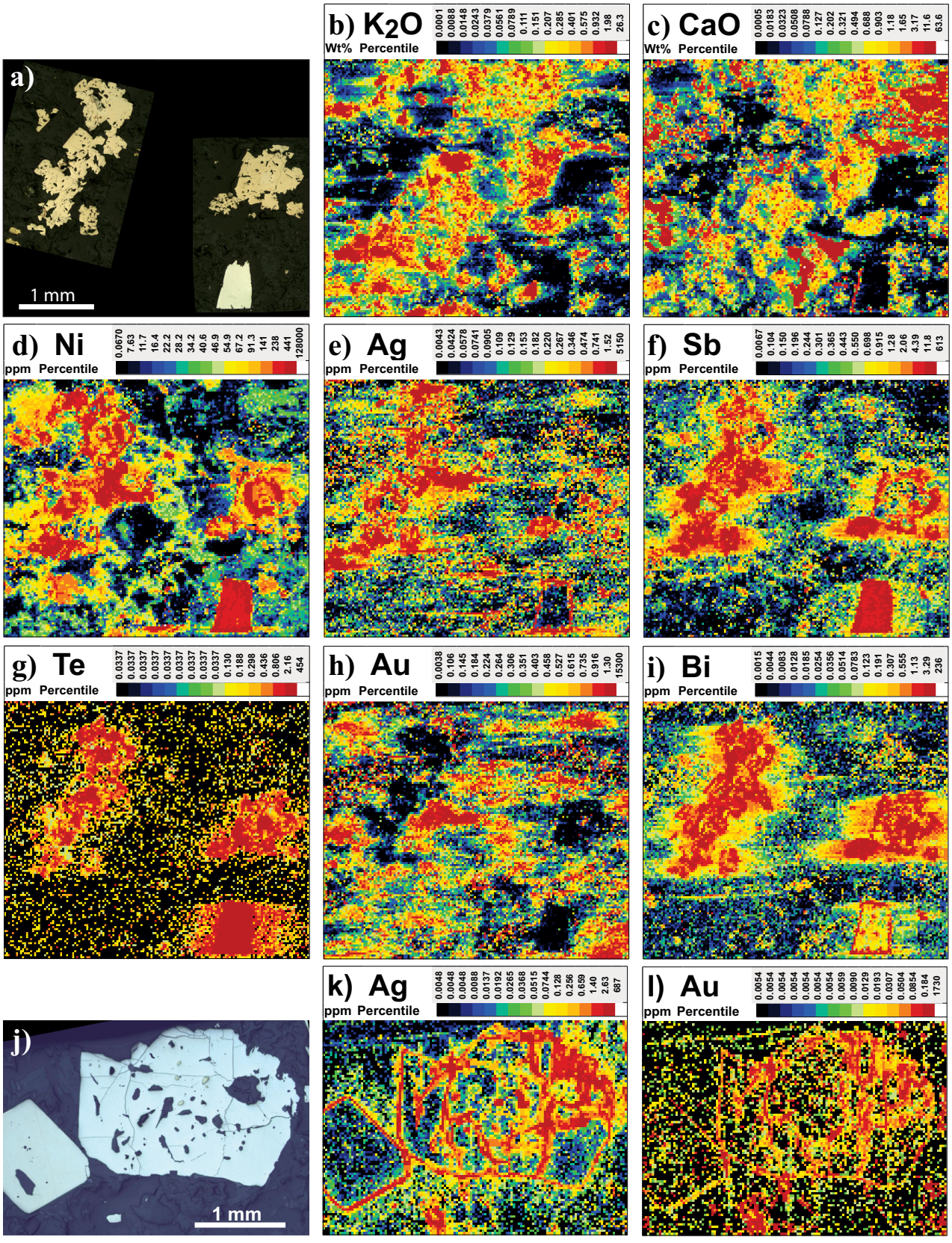


**Figure 6.** Photomicrograph and element concentration maps for two pyrite samples, CL13 (a-i) and CL10 (j-l) from the Côté Gold deposit. The sulphides in sample CL13 are pyrite (beige) and arsenopyrite (white). The sulphide in sample CL10 is pyrite. Scales are in ppm, with the exception of $K_2O$ and CaO, which are in weight percent. Elemental maps show that gold is depleted in pyrite and arsenopyrite, but locally enriched in silicate minerals (quartz, biotite, and chlorite). In sample CL10, gold and other metals are locally enriched in fractures in pyrite, indicating late introduction or remobilization.

in silicate-rich banded iron formation and occurs in association with stratabound pyrrhotite replacements and silica flooding, with local discordant quartz± pyrrhotite veins. The ore zones are associated with $D_2$ high-strain zones that are preferentially developed along hinges and strongly attenuated fold limbs of tight $F_2$ folds (e.g. Biczok et al., 2012; Oswald et al., 2014, 2015).

This study focussed particularly on mapping diagenetic pyrite nodules in argillaceous sedimentary rocks from the mine area. The nodules range from millimetre to centimetre in size and frequently show concentric zoning that is accentuated locally by inclusions. The nodules show variable degrees of recrystallization to pyrrhotite and inclusion-free subhedral-euhedral pyrite, mostly at their margins but also as patches within the nodules. These features are interpreted to be the products of nodule recrystallization during metamorphism.

LA-ICP-MS element maps of selected elements in the nodules and secondary pyrrhotite and pyrite are presented in Figures 7 and 8. Element maps reveal significant enrichment of Co, Ni, As, Se, Ag, Sb, Te, Au, Tl, Pb, and Bi in the pyrite nodules. All elements show flattened concentric zoning, indicative of syngenetic metal incorporation. The zoning is often truncated by recrystallized pyrite and pyrrhotite. Gold values typically range between 20 and 50 ppb but are locally up to >1 ppm in Au-rich growth zones in the nodules. Also notable is that patches of the dark carbonaceous alumino-silicate-rich sediment matrix contain spotty Au enrichment at concentrations frequently >2 ppm. Indeed, the average Au content of the non-sulphide material in Figure 7 is ~1 ppm.

Gold and most metals (Sb, Te, Ag, Pb, Bi) are strongly depleted in recrystallized pyrrhotite and pyrite. Arsenic is variably enriched in recrystallized pyrite and Se and Ni are enriched in pyrrhotite (>200 ppm) but depleted in recrystallized pyrite (mostly <20 ppm).

Element maps of Musselwhite ore samples (Fig. 8) show that Au occurs largely in quartz and in microfractures in pyrrhotite, and, to a lesser degree, in fractures in garnet (Moran, 2008; Kolb, 2011; Biczok et al., 2012).

In an effort to determine the relationship, if any, between the metals concentrated in diagenetic sulphide nodules and Musselwhite ore, Pb-isotope ratios, $^{207}Pb/^{206}Pb$ and $^{208}Pb/^{206}Pb$, were mapped in a Musselwhite diagenetic pyrite nodule and a small area of relatively Pb-rich ore (Fig. 8). Mean Pb-isotope ratios for areas of representative values within the nodule and ore samples are indistinguishable within the uncertainty of the measurements.

# DISCUSSION

## Occurrence of Gold

Pyrite (and arsenopyrite) is one of the most common sulphide minerals associated with gold-ore assemblages, in which gold commonly occurs as sulphide lattice-bound gold or nanoparticle inclusions (Deditius et al., 2011; Hough et al., 2011; Cook et al., 2013). Auriferous pyrite at Canadian Malartic and auriferous nodular sedimentary pyrite at Musselwhite, although of different origin, have relatively uniform gold distribution, suggesting that Au partitions into the sulphide as lattice-bound Au. Almost all pyrite grains from the Côté Gold deposit are depleted in Au, but silicate minerals (quartz, biotite, chlorite) are locally enriched in Au (>0.5 ppm) with a spotty distribution, which suggests that Au occurs as nanoparticles in these minerals. This unusual occurrence of Au warrants further investigation (e.g. high-resolution TEM studies) to better characterize its localization in the silicate minerals. Similar spotty Au enrichment in carbonaceous material at Musselwhite suggests a nanoparticulate mode for some of this Au. Gold in the Musselwhite ores occurs largely in quartz and in association with pyrrhotite and garnet, although it appears largely as enrichments along micro-fractures.

In summary, LA-ICP-MS mapping has revealed that Au in the three deposits studied occurs either visibly in quartz, as lattice-bound Au in pyrite, as fracture-bound in pyrrhotite and garnet, and as nanoparticle inclusions in silicate minerals and carbonaceous sediments.

## Evolution of the Hydrothermal Systems

Most gold mineralization-related elements, including Cu, Zn As, Ag, Sb, Te, W, Hg, Pb, and Bi, partition into pyrite. Thus, the distribution of elements in pyrite provides a record of the evolving composition and physico-chemistry of the hydrothermal fluids, which are very important for understanding the processes involved in the formation of the deposit and, as such, help define geological and exploration models. However, although elemental distributions within pyrite show significant potential for better understanding and perhaps isolating chemical trends that are prerequisite for gold mineralization, the behaviours of elements during pyrite crystallization (and recrystallization) are still poorly known due to the lack of supporting experimental data. For example, Ni and Co frequently show dramatic variations in concentrations during pyrite growth, the significance of which is largely unknown. The following interpretations are thus of an empirical nature based on our observations.

At the Canadian Malartic deposit, textural and quantitative elemental mapping has revealed five morphological and chemically distinct types of pyrite, which

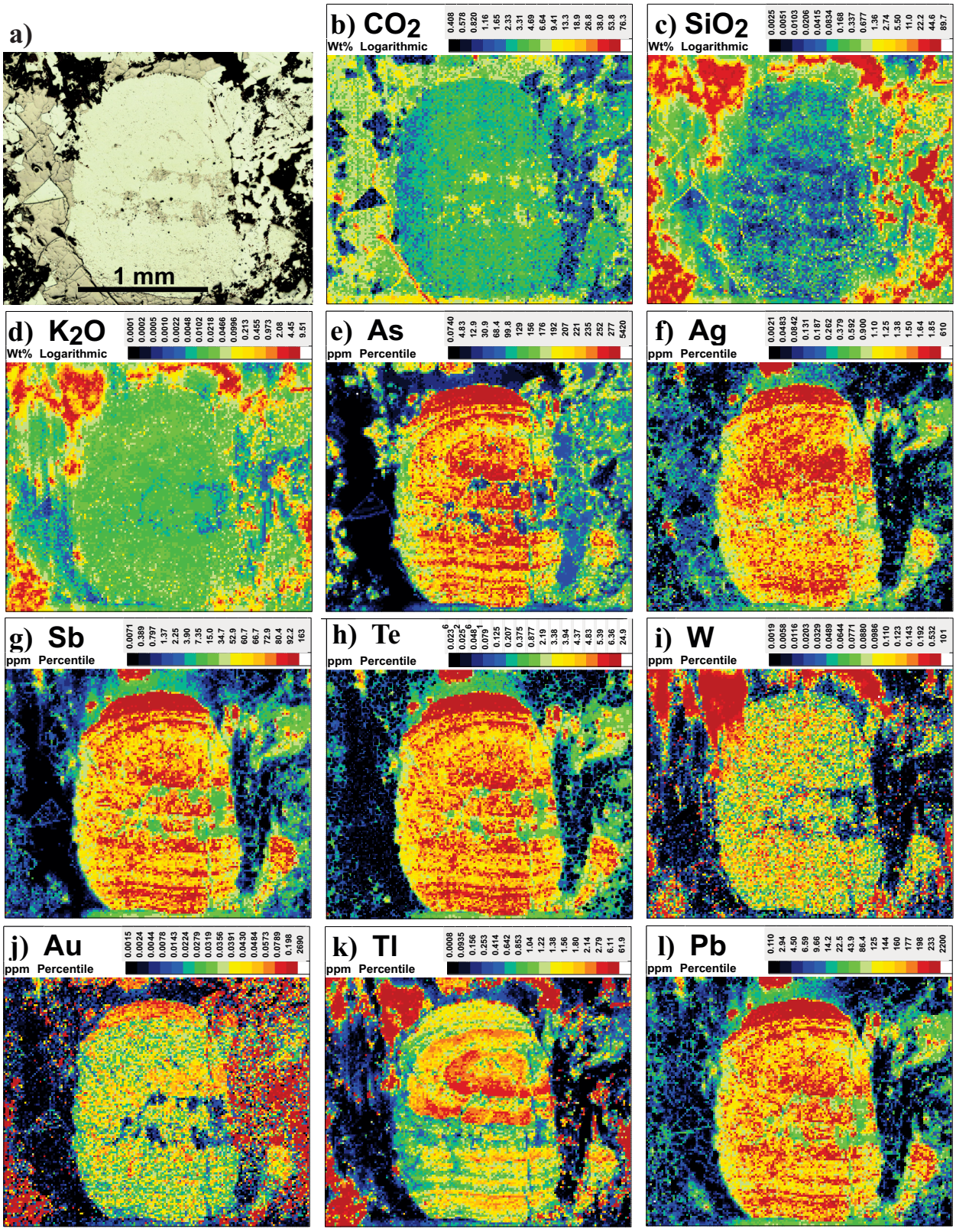


**Figure 7.** Photomicrograph and element concentration maps for a diagenetic pyrite nodule from sedimentary rocks in the vicinity of the Musselwhite deposit. Scales are in ppm, with the exception of $K_2O$ and CaO, which are in weight percent. The element maps reveal concentric enrichment of metals in the nodule. Zoning is truncated by recrystallized pyrite (white, crystalline) and pyrrhotite (pink-brown) around and within the nodule. Also notable are patches of the dark carbonaceous alumino-silicate-rich sediment matrix that contain spotty Au enrichment in concentrations that are frequently >2 ppm. Gold and most metals (Ag, Sb, Te, Pb, Bi) are strongly depleted in recrystallized pyrrhotite and pyrite. A narrow vein in the pyrite nodule provides evidence for generation of an auriferous fluid during internal recrystallization of pyrite to pyrrhotite.

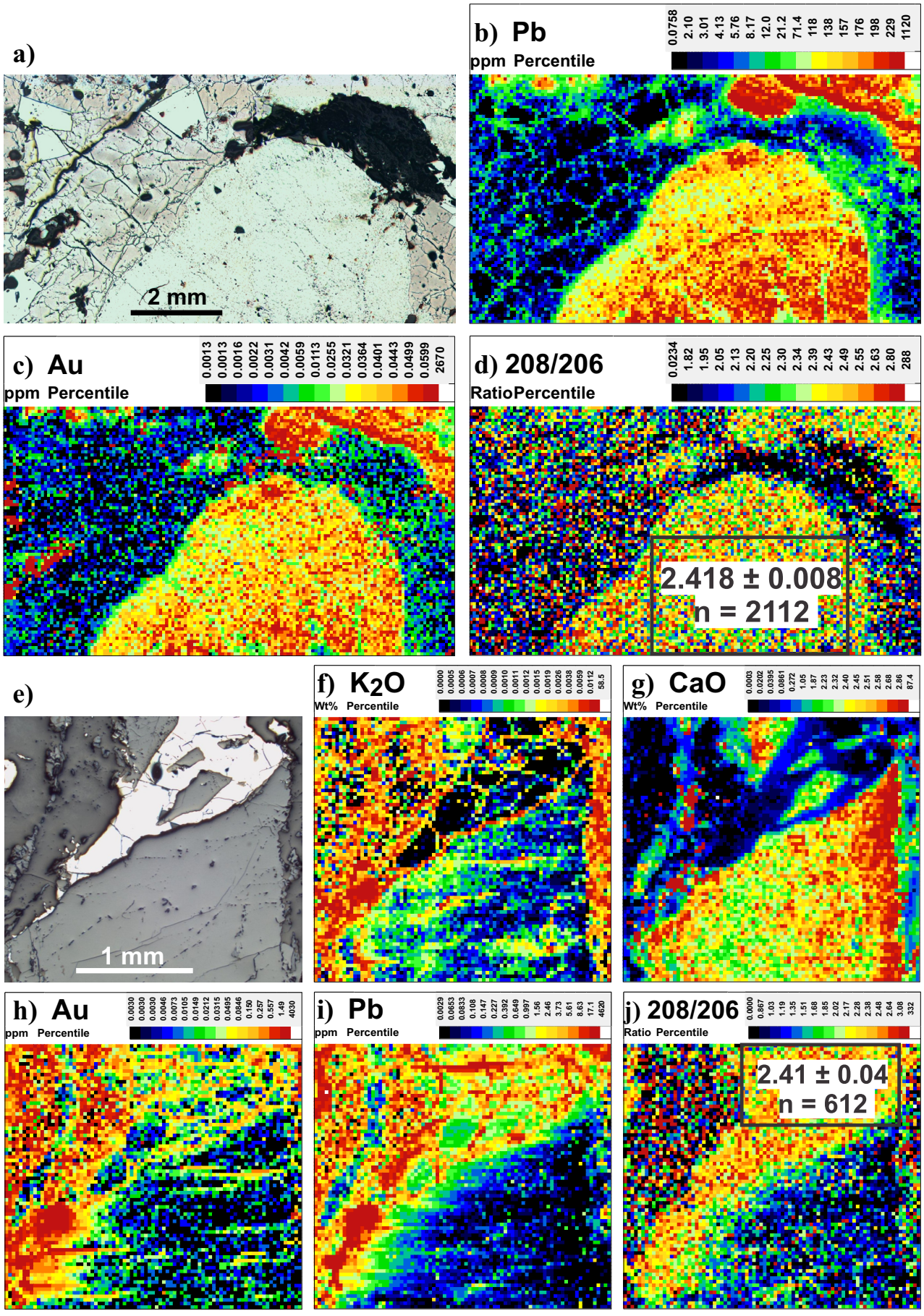
a)
2 mm
b) Pb
ppm Percentile
0.0758 2.10 3.01 4.13 5.76 8.17 12.0 21.2 71.4 118 138 157 176 198 229 1120
c) Au
ppm Percentile
0.0013 0.0013 0.0016 0.0022 0.0031 0.0042 0.0059 0.0113 0.0255 0.0321 0.0364 0.0401 0.0443 0.0499 0.0599 2670
d) 208/206
RatioPercentile
0.0234 1.82 1.95 2.05 2.13 2.20 2.25 2.30 2.34 2.39 2.43 2.49 2.55 2.63 2.80 288
2.418 ± 0.008
n = 2112
e)
1 mm
f) K2O
Wt% Percentile
0.0000 0.0005 0.0006 0.0007 0.0008 0.0009 0.0010 0.0011 0.0012 0.0015 0.0019 0.0026 0.0038 0.0059 0.0112 58.5
g) CaO
Wt% Percentile
0.0003 0.0202 0.0395 0.0861 0.272 1.05 1.87 2.23 2.32 2.40 2.45 2.51 2.58 2.68 2.86 87.4
h) Au
ppm Percentile
0.0030 0.0030 0.0030 0.0046 0.0073 0.0105 0.0149 0.0212 0.0315 0.0495 0.0846 0.150 0.257 0.557 1.49 4030
i) Pb
ppm Percentile
0.0029 0.0053 0.0833 0.108 0.147 0.227 0.392 0.649 0.997 1.56 2.46 3.73 5.61 8.63 17.1 4620
j) 208/206
Ratio Percentile
0.0000 0.867 1.03 1.19 1.35 1.51 1.68 1.85 2.02 2.17 2.28 2.38 2.48 2.64 3.08 332
2.41 ± 0.04
n = 612

are interpreted as related to three main stages of growth: (1) porous pyrite (py1), likely diagenetic pyrite, formed pre-mineralization; (2) Au-rich pyrite (py2–py4) crystallized during gold precipitation; each is enriched in Ag, Te, Au, Pb, and Bi and, in the latter part of this gold mineralization stage (py3, py4), Mo. Py3 and py4 are locally enclosed by, and/or contain inclusions of, K-rich silicate(s), suggesting that both precipitated from a K-rich fluid. This is consistent with, though not unequivocal evidence of, an intrusion-related magmatic-hydrothermal origin. After pyrite precipitation, there is evidence in the Sladen Fault zone for a post-pyrite fracture-related enrichment process associated with Ca-rich metasomatism, which may represent a syndeformational hydrothermal overprint.

Pyrite and arsenopyrite from the Côté Gold deposit are extremely depleted in Au; the Au enrichment occurs largely in hydrothermal silicate minerals (quartz, biotite, and chlorite) as possible nanoparticles of Au. Gold is also locally enriched in fractures cutting pyrite. These features suggest that gold mineralization in the breccia zone at the contact of tonalite and diorite mostly postdates pyrite crystallization, arguing for a relatively «late» introduction of Au. Later stage quartz-carbonate-pyrite veins in the deposit also often contain visible gold and have a high Au grade. However, the close spatial and temporal overlap of magmatic and hydrothermal events at Côté Gold argue strongly for a ca. 2,740 Ma magmatic-hydrothermal origin for the gold mineralization (Kontak et al., 2013; Katz et al., 2015). Based on these observations, it is suggested that gold mineralization at Côté Gold was the product of auriferous hydrothermal fluids released late in the evolution of the magmatic-hydrothermal system.

Element mapping of pyrite nodules in carbonaceous argillite at Musselwhite provide striking evidence for generation of Au-rich fluids during recrystallization and with similar element enrichments and Pb isotopic composition to the ore. This is discussed below.

## Source of Gold

Archean greenstone-hosted orogenic gold deposits constitute one of the most important types of gold deposit; however, their origin and in particular, the source of gold remains controversial (e.g. Goldfarb et al., 2005). Most models for orogenic gold deposits propose a deep source for the Au; for example, the mantle, deep magmas, or deep crust. In the latter case, auriferous fluid was generated during prograde amphibolite- or granulite-facies metamorphism of subducted volcano-sedimentary terranes during accretionary or collisional tectonics (Kerrich et al., 2000; Goldfarb et al., 2005; Dubé and Gosselin, 2007). Recently, however, increasingly compelling evidence has been presented that gold in at least some orogenic, metasedimentary rock-hosted deposits is derived more locally from organic- and pyrite-rich shale in the host sedimentary basin during progressive diagenesis and metamorphism. Particularly, strong support has been provided by detailed LA-ICP-MS and fluid inclusion studies on a number of deposits (Large et al., 2007, 2009, 2011; Meffre et al., 2008; Thomas et al., 2011; Gaboury, 2013; Steadman et al., 2013, 2014; Bull and Large, 2014). These studies support a two-stage model for generation of some orogenic gold deposits: (1) Au, As, and other metals are introduced early into black shale and turbidite basins and are concentrated into early diagenetic arsenian pyrite; (2) during diagenesis and early metamorphism, the diagenetic pyrite is recrystallized to form coarser grained pyrite. Under higher grade metamorphism (lower greenschist facies and above) the arsenian pyrite is converted to pyrrhotite. These processes release Au, As, S, and other elements into a fluid phase, which is channelled into structural sites, such as shear zones and fold hinges, within or above the black shale sequence and precipitated by chemical reaction with reactive host rocks. Large et al. (2011) proposed that argillite beds with invisible Au contents of greater than 250 ppb in diagenetic pyrite were potential source rocks for economic gold deposits.

The sedimentary country rocks in the Musselwhite deposit area contain auriferous diagenetic pyrite. The following assesses the evidence that element mapping can provide answers as to whether these sedimentary units are one potential source of Au in these deposits. Three questions are addressed:

1. Is there evidence of auriferous diagenetic sulphides undergoing recrystallization and Au loss? The striking diagenetic pyrite nodules and carbonaceous lenses in argillite from Musselwhite locally contain >1 ppm Au, together with elevated concentrations of As, Mo, Ag, Sb, Te, W, Tl, Pb, and Bi. The con-

**Figure 8 (opposite page).** Photomicrographs and element concentration and Pb-isotope maps of a pyrite nodule and Pb-rich Au ore, Musselwhite deposit. **a)** Reflected light photomicrograph of a pyrite nodule in recrystallized sulphides, pyrrhotite (pink brown) and pyrite (white). **b, c)** Pb and Au concentration maps. **d)** $^{208}Pb/^{206}Pb$ map with mean ± uncertainty (2 S.E.) for rectangular area shown. **e)** Reflected light photomicrograph of gold ore showing quartz (darker grey), garnet (lighter grey), and pyrrhotite (white). **f–i)** $K_2O$, CaO, Au, and Pb concentration maps. **j)** $^{208}Pb/^{206}Pb$ map with mean ± uncertainty (2 S.E.) for rectangular area shown. Concentration scales are in ppm, with the exception of $K_2O$ and CaO, which are in weight percent. Note that Pb and Au in the ore are concentrated largely in quartz and within fractures in pyrrhotite, suggesting likely co-precipitation. The mean Pb isotope value of the highlighted rectangular area of pyrrhotite (8f), chosen for its relatively consistent values, agrees within uncertainty with the pyrite nodule value (8d).

centric zonation of metal enrichments in the nodules is consistent with a syngenetic origin of metal concentration. By contrast, recrystallized pyrite and pyrrhotite are depleted in these elements. This is strikingly displayed in Figure 7, which shows a zone of incipient pyrrhotite recrystallization within a diagenetic pyrite nodule. The recrystallized zone is depleted in all metals, and even K, relative to the nodule, with the exception of Ni and Se, which are strongly sequestered by pyrrhotite. A narrow fracture through the nodule shows Au depletion (a gold-poor fluid entering the nodule?) to one side of the pyrrhotite and Au enrichment on the other side (a Au-rich fluid exiting the nodule?). This map provides strong evidence of Au and other metal remobilization and entrainment in a fluid during sulphide recrystallization.

Importantly, there are also spotty but strong enrichments of Au in the carbonaceous sedimentary matrix to the nodule. In fact, the matrix to the nodule has a mean Au content greater than 10 times the Au content of the nodule. Only Mo and W are similarly concentrated. The source and timing of introduction of this Au in the matrix are unclear but it appears to be Au sequestered by organic material. The carbon-associated gold greatly increases the potential of this rock to have been a Au source rock.

2. Is there evidence to link the metals in the diagenetic sulphides to the Au in the deposits? Figure 8 shows that Pb-isotope values for a nodule (100s ppm Pb) and Pb-rich (10s ppm) gold ore are indistinguishable within the uncertainties of the analyses. The close spatial relationship of Pb and Au enrichment in the ore clearly supports co-precipitation of the metals. This information is consistent with Musselwhite Pb, and by inference, at least some of the Au, being derived from the pyritic carbonaceous sedimentary rocks.
3. Is there sufficient pyritiferous carbonaceous argillite in the sedimentary basin at Musselwhite to provide the gold in the deposit? Pyritiferous shale units are a much richer potential source of Au than typical greenstones and porphyries. Our calculations show that a fluid extracting Au, with an efficiency of 50%, from as little as ~0.5 km$^3$ of argillite containing 0.1 ppm Au (e.g. a 5 km square layer(s) of argillite totalling 60 m thick) could have provided all of the ~6 Moz of Au at Musselwhite. The exposed thickness of pyritiferous argillite at Musselwhite totals only a few metres (Oswald et al., 2015). However, if additional layers exist at depth, they could potentially have made a significant contribution to the Au contained in the Musselwhite deposit.

Pre-mineralization pyrite at Canadian Malartic is poor in Au (~0.1 ppm) and is not likely to have been an important source for gold. Some Au-enriched pyrite at Canadian Malartic (py3 and py4) is associated with potassic alteration and elevated levels of Mo, consistent with deposition in a magmatic-hydrothermal system. Similarly, the Côté Gold deposit, which is hosted in magmatic and hydrothermal breccia, and where Au occurs in magmatic-hydrothermal silicate alteration minerals, is inferred to have been deposited from magmatic-hydrothermal fluids, although late in the evolution of the system.

Thus, the deposits that were studied have multiple gold sources: magmatic fluids were likely important at Côté Gold and Canadian Malartic, with metamorphic fluids, perhaps remobilizing early magmatic hydrothermal Au, potentially important at Canadian Malartic (De Souza et al., 2015), and Au derived, at least in part, from local pyritic, carbonaceous argillite, potentially important at Musselwhite.

## IMPLICATIONS FOR EXPLORATION

Elemental mapping of pyrite and associated minerals can be helpful in fingerprinting the type of gold occurrence, the distribution of Au within the ores, and identifying potentially fertile sedimentary source rocks. In this study, we found that Au partitions strongly into pyrite and thus, as historically known, pyrite Au content is a generally good indicator of gold mineralization (e.g. Amaro et al., 1988). Pyrite in the samples studied from the Côté Gold deposit does not contain economic concentrations of Au; Au is, rather, hosted dominantly in silicate alteration minerals. The Musselwhite deposit is a BIF-hosted pyrrhotite-rich replacement-style gold deposit hosted in a volcano-sedimentary package that contains carbonaceous argillite-bearing auriferous diagenetic pyrite. In this type of gold deposit, carbonaceous shale and, especially, Au-rich diagenetic sulphide nodules in the sedimentary sequence, is potentially a regional-scale first-order indicator of potentially fertile exploration terrain (e.g. Large et al., 2009).

## FUTURE WORK

The near-ubiquitous occurrence of pyrite in association with Au deposits and its demonstrated ability to concentrate elements and record the chemical history of its source hydrothermal system(s), and thus act as a vector to hidden mineralization, reinforces the evidence that pyrite chemistry requires further investigation. Future studies will concentrate on modelling element distributions in pyrite to determine compositional evolutionary fingerprints of productive systems and to develop chemical criteria of system fertility.

Because of its exploration significance, the connection between early Au enrichment in pyritic carbona-

ceous argillite and orogenic Au deposits requires much further investigation. Further work is currently in progress on diagenetic sulphide nodules in argillite using historical samples from the Hollinger-McIntyre and Owl Creek mines, Timmins.

Also still being evaluated are LA-ICP-MS data on zircon grains from the Côté Gold and Canadian Malartic gold deposits, which will provide important constraints on the oxidation state of the associated intrusions.

In situ isotopic compositions (e.g. Fe and S isotopes) of pyrite and other sulphides can provide potential constraints on the physico-chemistry of fluids/melts. Data collected from a Fe-isotope study of pyrite from the Côté Gold deposit are currently being evaluated. Furthermore, most Au deposits in the Abitibi greenstone belt have associated Ag and Te enrichments, so the stable isotopes of these metals may provide evidence to the source of Au and should be investigated in future studies, especially if combined with in situ elemental mapping and S- and Fe-isotope analyses.

## ACKNOWLEDGEMENTS

This is a contribution to the Targeted Geoscience Initiative 4 (TGI-4) (2010-2015). We wish to thank Mine Canadian Malartic, Goldcorp, and Iamgold for supporting this study. Jian-Feng Gao thanks NSERC for the award of a visiting fellowship to the GSC. Dr. Zhaoping Yang's assistance with LA-ICP-MS analytical work and data processing is much appreciated.

## REFERENCES

Agangi, A., Hofmann, A., and Wohlgemuth-Ueberwasser, C.C., 2013. Pyrite zoning as a Record of Mineralization in the Ventersdorp Contact Reef, Witwatersrand Basin, South Africa; Economic Geology, v. 108, p. 1243–1272.

Amaro, D., Ho, S., Groves, D., McNaughton, N., Dahl, N., Poll, N., and Grigson, M., 1988. The use of pyrite as an indicator of Archaean gold mineralization processes: examples from Western Australia, *In:* Abstracts; Bicentennial Gold 88, Geological Society of Australia, v. 23, p. 414–418.

Biczok, J., Hollings, P., Klipfel, P., Heaman, L., Maas, R., Hamilton, M., Kamo, S., and Friedman, R., 2012. Geochronology of the North Caribou greenstone belt, Superior Province Canada: Implications for tectonic history and gold mineralization at the Musselwhite mine; Precambrian Research, v. 192-195, p. 209–230.

Bull, S.W. and Large, R.R., 2014. Setting the stage for the genesis of the giant Bendigo ore system, *In:* Ore Deposits in an Evolving Earth, (ed.) G.R.T. Jenkin, P.A.J. Lusty, I. McDonald, I., M.P. Smith, A.J. Boyce, and J.J. Wilkinson; Geological Society of London, Special Publication No. 393, p. 1–31.

Chouinard, A., Paquette, J., and Williams-Jones, A.E., 2005. Crystallographic controls on trace-element incorporation in auriferous pyrite from the Pascua epithermal high-sulphidation deposit, Chile-Argentina; The Canadian Mineralogist, v. 43, p. 951–963.

Cook, N.J. and Chryssoulis, S.L., 1990. Concentrations of invisible gold in the common sulfides; The Canadian Mineralogist, v. 28, p. 1–16.

Cook, N.J., Ciobanu, C.L., Meria, D., Silcock, D., and Wade, B., 2013. Arsenopyrite-Pyrite Association in an Orogenic Gold Ore: Tracing Mineralization History from Textures and Trace Elements; Economic Geology, v. 108, p. 1273–1283.

Deditius, A.P., Utsunomiya, S., Reich, M., Kesler, S.E., Ewing, R.C., Hough, R., and Walshe, J., 2011. Trace metal nanoparticles in pyrite; Ore Geology Reviews, v. 42, p. 32–46.

Deol, S., Deb, M., Large, R.R., and Gilbert, S., 2012. LA-ICPMS and EPMA studies of pyrite, arsenopyrite and loellingite from the Bhukia-Jagpura gold prospect, southern Rajasthan, India: Implications for ore genesis and gold remobilization; Chemical Geology, v. 326-327, p. 72–87.

De Souza, S., Dubé, B., McNicoll, V.J., Dupuis, C., Mercier-Langevin, P., Creaser, R.A., and Kjarsgaard, I.M., 2015. Geology, hydrothermal alteration, and genesis of the world-class Canadian Malartic stockwork-disseminated Archean gold deposit, Abitibi, Quebec, *In:* Targeted Geoscience Initiative 4: Contributions to the Understanding of Precambrian Lode Gold Deposits and Implications for Exploration, (ed.) B. Dubé and P. Mercier-Langevin; Geological Survey of Canada, Open File 7852, p. 113–126.

De Souza, S., Dubé, B., McNicoll, V., Dupuis, C., Mercier-Langevin, P., Creaser, R., and Kjarsgaard, I., in press. Geology, structure and timing of hydrothermal alteration at the Canadian Malartic Archean stockwork disseminated world-class gold deposit, Quebec, Canada, *In:* Archean Base and Precious Metal Deposits, Southern Abitibi Greenstone Belt, Canada, (eds.) T. Monecke, P. Mercier-Langevin, and B. Dubé; Society of Economic Geologists, Field Guide Book 46.

Dubé, B. and Gosselin, P., 2007. Greenstone-hosted quartz-carbonate vein deposits, *In:* Mineral Deposits of Canada: A Synthesis of Major Deposit Types, District Metallogeny, the Evolution of Geological Provinces and Exploration Methods, (ed.) W.D. Goodfellow; Geological Association of Canada, Mineral Deposits Division, Special Publication No. 5, p. 49–73.

Dubé, B., Gosselin, P., Mercier-Langevin, P., Hannington, M., and Galley, A., 2007. Gold-rich Volcanogenic Massive Sulphide Deposits, *In:* Mineral Deposits of Canada: A Synthesis of Major Deposit Types, District Metallogeny, the Evolution of Geological Provinces and Exploration Methods, (ed.) W.D. Goodfellow; Geological Association of Canada, Mineral Deposits Division, Special Publication No. 5, p. 45–94.

Gaboury, D., 2013. Does gold in orogenic deposits come from pyrite in deeply buried carbon-rich sediments?: Insight from volatiles in fluid inclusions; Geology, v. 41, p. 1207–1210.

Goldfarb, R.J., Baker, T., Dubé, B., Groves, D.I., Hart, C.J.R., and Gosselin, P., 2005. Distribution, character, and genesis of gold deposits in metamorphic terranes, *In:* Economic Geology 100th Anniversary Volume, (ed.) J.W. Hedenquist, J.F.H. Thompson, R.J. Goldfarb, and J.P. Richards; Society of Economic Geologists, Littleton, Colorado, p. 407–450.

Halicz, L. and Günther, D., 2004. Quantitative analysis of silicates using LA-ICP-MS with liquid calibration; Journal of Analytical Atomic Spectrometry, v. 19, p. 1539–1545.

Heather, K.B. and van Breemen, O., 1994. An interim report on geological, structural, and geochronological investigations of granitoid rocks in the vicinity of the Swayze greenstone belt, southern Superior Province, Ontario, *In:* Canadian Shield; Geological Survey of Canada, Current Research 1994-C, p. 259–268.

Heather, K.B., Shore, G.T., and van Breemen, O., 1996. Geological investigations in the Swayze greenstone belt, southern Superior Province, Ontario: a final update, *In:* Canadian Shield;

Geological Survey of Canada, Current Research 1996-C, p. 125–136.

Heather, K.B. and Shore, G.T., 1999a. Geology, Swayze Greenstone Belt, Ontario; Geological Survey of Canada, Open File 3384a, sheet 2, scale 1:50 000.

Heather, K.B. and Shore, G.T., 1999b. Geology, Gogama, Swayze Greenstone Belt, Ontario; Geological Survey of Canada, Open File 3384g, scale 1:50 000.

Heather, K.B., 2001. The geological evolution of the Archean Swayze Greenstone Belt, Superior Province, Canada; Ph.D. thesis, Keele University, Keele, England, 370 p.

Hodgson, C.J. and MacGeehan, P.J., 1982. Geological characteristics of gold deposits in the Superior Province of the Canadian Shield, *In:* Geology of Canadian Gold Deposits, (ed.) R.W. Hodder and W. Petruks; Canadian Institute of Mining and Metallurgy, Special Volume 24, p. 211–229.

Hough, R.M., Noble, R.R.P., and Reich, M., 2011. Natural gold nanoparticles; Ore Geology Reviews, v. 42, p. 55–61.

Jackson, S.E., 2008. LAMTRACE data reduction software for LA-ICP-MS, *In:* Laser Ablation-ICP-Mass Spectrometry in the Earth Sciences: Current Practices and Outstanding Issues, (ed.) P. Sylvester; Mineralogical Association of Canada, Short Course Series, v. 40, p. 305–307.

Katz, L.R., Kontak, D.J., Dubé, B., and McNicoll, V.J., 2015. The Archean Côté gold intrusion-related Au(-Cu) deposit, Ontario, Canada: A large-tonnage, low-grade deposit centred on a magmatic-hydrothermal breccia, *In:* Targeted Geoscience Initiative 4: Contributions to the Understanding of Precambrian Lode Gold Deposits and Implications for Exploration, (ed.) B. Dubé and P. Mercier-Langevin; Geological Survey of Canada, Open File 7852, p. 139–155.

Kerrich, R., Goldfarb, R., Groves, D., and Garwin, S., 2000. The geodynamics of world-class gold deposits: characteristics, space-time distribution and origins, *In:* Gold in 2000, (ed.) S.G. Hagemann and P.E. Brown; Society of Economic Geologists, Reviews in Economic Geology, v. 13, p. 501–551.

Kolb, M., 2011. A microstructural study of Musselwhite Mine and Hammond Reef shear-zone-hosted gold deposits; M.Sc. thesis, Lakehead University, Thunder Bay, Ontario, 204 p.

Koglin, N., Frimmel, H., Lawrie Minter, W.E., and Brätz, H., 2010. Trace-element characteristics of different pyrite types in Mesoarchaean to Palaeoproterozoic placer deposits; Mineralium Deposita, v. 45, p. 259–280.

Kontak, D.J., Creaser, R.A., and Hamilton, M., 2013. Geological and geochemical studies of the Côté Lake Au(-Cu) deposit Area, Chester Township, Northern Ontario, *In:* Results from the Shining Tree, Chester Township and Matachewan Gold Projects and the Northern Cobalt Embayment Polymetallic Vein Project, (ed.) J.A. Ayer, D.J. Kontak, R.L. Linnen, and S. Lin; Ontario Geological Survey, Miscellaneous Release Data 294.

Large, R.R., Bull, S.W., and Maslennikov, V.V., 2011. A Carbonaceous Sedimentary Source-Rock Model for Carlin-Type and Orogenic Gold Deposits; Economic Geology, v. 106, p. 331–358.

Large, R.R., Danyushevsky, L., Hollit, C., Maslennikov, V., Meffre, S., Gilbert, S., Bull, S., Scott, R., Emsbo, P., Thomas, H., Singh, B., and Foster, J., 2009. Gold and Trace Element Zonation in Pyrite Using a Laser Imaging Technique: Implications for the Timing of Gold in Orogenic and Carlin-Style Sediment-Hosted Deposits; Economic Geology, v. 104, p. 635–668.

Large, R.R., Maslennikov, V.V., Robert, F., Danyushevsky, L.V., and Chang, Z., 2007. Multistage sedimentary and metamorphic origin of pyrite and gold in the Giant Sukhoi Log Deposit, Lena Gold Province, Russia; Economic Geology, v. 102, p. 1233–1267.

Large, R.R., Meffre, S., Burnett, R., Guy, B., Bull, S., Gilbert, S., Goemann, K., and Danyushevsky, L., 2013. Evidence for an intrabasinal source and multiple concentration processes in the formation of the Carbon Leader Reef, Witwatersrand Supergroup, South Africa; Economic Geology, v. 108, p. 1215–1241.

Meffre, S., Large, R.R., Scott, R., Woodhead, J., Chang, Z., Gilbert, S.E., Danyushevsky, L.V., Maslennikov, V., and Hergt, J.M., 2008. Age and pyrite Pb-isotopic composition of the giant Sukhoi Log sediment-hosted gold deposit, Russia; Geochimica et Cosmochimica Acta, v. 72, p. 2377–2391.

Mercier-Langevin, P., Dubé, B., Lafrance, B., Hannington, M., Galley, A., Moorhead, J., and Gosselin, P., 2007. Metallogeny of the Doyon-Bousquet-LaRonde Mining Camp, Abitibi Greenstone Belt, Quebec, *In:* Mineral Deposits of Canada: A Synthesis of Major Deposit Types, District Metallogeny, the Evolution of Geological Provinces and Exploration Methods, (ed.) W.D. Goodfellow; Geological Association of Canada, Mineral Deposits Division, Special Publication No. 5, p. 673–701.

Moran, P., 2008. Lithogeochemistry of the sedimentary stratigraphy and metasomatic alteration in the Musselwhite gold deposit. North Caribou Lake metavolcanic-metasedimentary belt, Superior Province, Canada: implications for deposition and mineralization; M.Sc. Thesis, Lakehead University, Thunder Bay, Ontario, 351 p.

Oswald, W., Castonguay, S., Dubé, B., Mercier-Langevin, P., Malo, M., Biczok, J., and McNicoll, V., 2014. Targeted Geoscience Initiative 4. Lode gold deposits in ancient deformed and metamorphosed terranes: detailed mapping of key stripped outcrops in the Musselwhite Mine area, Northwestern Ontario, and implications for the geological and structural setting of the gold mineralization, *In:* Summary of field work and other activities 2014; Ontario Geological Survey, Open File Report 6300, p. 42-1 to 42-15.

Oswald, W., Castonguay, S., Dubé, B., McNicoll, V.J., Biczok, J., Malo, M., and Mercier-Langevin, P., 2015. Geological setting of the world-class Musselwhite gold Mine, Superior Province, northwestern Ontario, and implications for exploration, *In:* Targeted Geoscience Initiative 4: Contributions to the Understanding of Precambrian Lode Gold Deposits and Implications for Exploration, (ed.) B. Dubé and P. Mercier-Langevin; Geological Survey of Canada, Open File 7852, p. 69–84.

Poulsen, K.H., Robert, F., and Dubé, B., 2000. Geological Classification of Canadian Gold Deposits; Geological Survey of Canada, Bulletin 540, 106 p.

Robert, F., Poulsen, K.H., Cassidy, K.F., and Hodgson, C.J., 2005. Gold metallogeny of the Superior and Yilgarn cratons, *In:* Economic Geology 100th Anniversary Volume, (ed.) J.W. Hedenquist, J.F.H. Thompson, R.J. Goldfarb, and J.P. Richards; Society of Economic Geologists, Littleton, Colorado, p. 1001–1033.

Steadman, J.A., Large, R.R., Meffre, S., and Bull, S.W., 2013. Age, origin and significance of nodular sulfides in 2680 Ma carbonaceous black shale of the Eastern Goldfields Superterrane, Yilgarn Craton, Western Australia; Precambrian Research, v. 230, p. 227–247.

Steadman, J.A., Large, R.R., Davidson, G.J., Bull, S.W., Thompson, J., Ireland, T. R., and Holden P., 2014. Paragenesis and composition of ore minerals in the Randalls BIF-hosted gold deposits, Yilgarn Craton, Western Australia: Implications for the timing of deposit formation and constraints on gold sources; Precambrian Research, v. 243, p. 110–132.

Thomas, H.V., Large, R.R., Bull, S.W., Maslennikov, V., Berry, R.F., Fraser, R., Froud, S., and Moye, R., 2011. Pyrite and

pyrrhotite textures and composition in sediments, laminated quartz veins, and reefs at Bendigo gold mine, Australia: insights for ore genesis; Economic Geology, v. 106, p. 1–31.

Woodhead, J.D., Hellstrom, J., Hergt, J.M., Greig, A., and Maas, R., 2007. Isotopic and elemental imaging of geological materials by laser ablation inductively coupled plasma-mass spectrometry; Geostandards and Geoanalytical Research, v. 31, p. 331–343.

Woodhead, J.D., Hellstrom, J., Paton, C., Hergt, J., Greig, A., and Maas, R., 2008. A guide to depth profiling and imaging applications of LA–ICP–MS; Mineralogical Association of Canada, Short Course Series, v. 40, p. 135–145.